Advanced Composites & Hybrid Materials

Accepted Manuscript

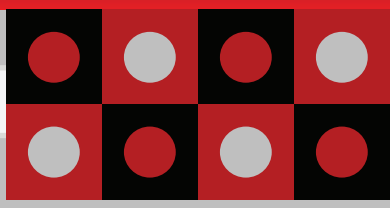

Strengthened electromagnetic absorption performance derived from synergistic effect of carbon nanotube hybrid with Co@C beads

Nannan Wu,[a] Jing Qiao,[a] Jiurong Liu,[a,*] Wenjing Du,[a] Dongmei Xu[b], and Wei Liu[b]

[a] Key Laboratory for Liquid-Solid Structural Evolution and Processing of Materials, Ministry of Education and School of Materials Science and Engineering, Shandong University, Jinan, Shandong 250061, People's Republic of China

[b] State Key Laboratory of Crystal Materials, Shandong University, Shandong 250100, China

*Corresponding author.

E-mail addresses: jrliu@sdu.edu.cn (J. Liu)

Tel: +86-531-88390236; Fax: +86-531-88392315

Abstract:

The composite structure of Co beads (200-300 nm) threaded by carbon nanotubes has been synthesized through a facile solvothermal method followed by a carbon reduction process. A carbon layer of ca. 5 nm was coated on the surface of Co beads to form a core-shell structure (CNTs/Co@C), in favor of the anti-oxidation of Co nanoparticles. The CNTs/Co@C hybrid showed a saturation magnetization (M_s) of 82.5 emu g^{-1} and a larger H_c value of 258.8 Oe than bulk Co (ca. 10 Oe). Served as an EM wave absorption material, the epoxy resin composites consisting of 60 wt% and 40 wt% CNTs/Co@C hybrid exhibited effective EM absorption (RL < -10 dB) over the frequency ranges of 1.5-15 GHz and 1.6-20 GHz with the matching thicknesses of 1.0-7.5 and 1.0-10.0 mm, respectively. The superior EM absorption performances of CNTs/Co@C hybrid containing strong absorption, wide frequency range, thin thickness, and light weight are mainly attributed to the synergy of magnetic loss from Co beads and dielectric loss from carbon nanotubes, as well as remarkable impedance matching.

KEYWORDS: composites, electromagnetic absorption, dielectric loss, magnetic loss

1. Introduction

Nowadays, electromagnetic interface (EMI) deriving from the rapid development of wireless devices and radar systems have drawn great interest in exploiting highly effective EM absorption materials to address serious EMI issues.[1-12] Generally, an ideal EM absorber should satisfy the requirements of light weight, strong absorption, wide absorption frequency range, and thin matching thickness. Depending on the attenuation mechanisms, the EM absorption materials can be mainly classified into two types: one is magnetic loss materials such as Fe,[13] Co,[14,15] Ni,[16,17] and ferrites,[1,18] while another is dielectric loss materials including CNTs,[19] CuS,[20] ZnO,[21] TiO_2,[22] etc. However, it is not facile to achieve impedance matching relying solely on dielectric loss or magnetic loss according to $Z_{in} = Z_0(\mu_r/\varepsilon_r)^{1/2}$.[23] In order to improve the impedance matching and gain efficient EM absorption properties, many efforts have been made to construct hybrids or composites, in which magnetic materials are elaborately incorporated with dielectric components, and examples include Fe_3O_4/SiO_2 nanorods,[5] Fe/SiO_2 nanocomposites,[24] FeNi@C nanocomposites,[25] SiC/Co nanowires[26] and so on. Nevertheless, the relatively high density and thick matching thickness of these magnetic/dielectric hybrids greatly restrict their practical applications. Based on the quarter-wavelength model ($t_m = nc/4f_m(\varepsilon_r\mu_r)^{1/2}$),[27] the enhanced permittivity and permeability values are beneficial to obtaining thin absorption thickness. As the development of new types of EM absorbers only by varying magnetic components and permeability is quite limited, much research attention has been directed towards finding innovative dielectric loss materials with

low density and high loss performance. Among various kinds of dielectric loss materials, carbon materials have always been attractive due to their low density, abundant resources, and low cost.[28-30] In particular, carbon nanotubes have been regarded as one competitive candidate based on their good conductivity, strong mechanical property, and high aspect ratio. Its large surface area and unique tubular morphology facilitate high loading of magnetic components, and meanwhile the superior electrical property promotes attenuation of incident EM wave. In the past years, some ferrites such as Fe_3O_4, $CoFe_2O_4$, have been frequently employed to serve as magnetic components in the magnetic CNTs hybrids.[31-33] In contrast with these traditional ferrites, magnetic metals (e.g., Fe, Co, Ni, and their alloys) own larger saturation magnetizations and higher Snoek's limits, which make them as better magnetic components for CNTs-based EM absorbers. For example, CNTs encapsulated with Fe/Co/Ni nanoparticles exhibited excellent EM absorption properties in S-band (2-4 GHz), mainly attributing to better matching of permeability and permittivity derived from magnetic nanoparticles and CNTs.[34] The hybrids of CNTs deposited by Ni nanoparticles showed an enhanced EM absorption capacity than pure CNTs at the same thickness, and achieved a minimal reflection loss of -11.5 dB at 3.4 GHz.[35] According to the previous researches, magnetic metal nanoparticles/CNTs hybrid materials can be mainly divided into two categories, in which magnetic metal nanoparticles are either encapsulated into the cavity of CNTs or deposited onto CNTs surface. The first type shows that only a limited amount of magnetic nanoparticles can be loaded into CNTs, making the permeability of hybrids

hard to improve. As for the second type, the magnetic metal nanoparticles deposited on the CNTs surface are liable to be oxidized and induced the enhancement of spin disorder, resulting in the reduction of ferromagnetism and permeability. Besides, the reported methods that were applied to prepare magnetic metal nanoparticles/CNTs hybrid materials include irradiative rays,[35] dc-arc discharge,[36] CVD,[37] and electro-plating,[38] which need high-energy input, special devices or complicated procedures.

Inspired by the previous researches, in this work, a composite of Co beads (200-300 nm) threaded by carbon nanotubes has been synthesized through a facile solvothermal route followed by a carbon reduction process. Meanwhile, a carbon layer of ca. 5 nm was coated on the surface of Co beads to form a core-shell structure (CNTs/Co@C), which is in favor of anti-oxidation of Co nanoparticles. Benefited from the synergy of high magnetic loss from Co beads and dielectric loss from CNTs, the as-synthesized CNTs/Co@C hybrid displayed superior EM absorption performances with strong absorption intensity, thin thickness, and broad bandwidth. Moreover, the presence of multi-interfaces among CNTs/Co@C hybrid, are also beneficial for the enhancement of EM absorption.

2. Experimental section

2.1 Chemicals

Cobalt nitrate hexahydrate ($Co(NO_3)_2 \cdot 6H_2O$) and pyrrole (C_4H_5N) were supplied by Sinopharm Chemical Reagent Co. Ltd. All chemicals were analytical grade and used without further purification. Carbon nanotubes (CNTs, length 5-15 μm, diameter

20-50 nm) were purchased from Shenzhen Nanotech Port Co. Ltd. They were purified and mildly treated for use according to our previous works.

2.2 Synthesis of beaded CNTs/Co_3O_4 hybrids

To synthesize the CNTs/Co@C hybrid, the CNTs/Co_3O_4 composite was firstly prepared as intermediate through a solvothermal method. In a typical experiment, 1 mmol $Co(NO_3)_2 \cdot 6H_2O$ was dissolved in 10 ml ethanol with magnetic stirring to form a red solution. Then, 0.01 g acid-treated CNTs were added in the above solution under ultrasonic treatment for 30 min. The resulting mixture was transferred into a 30 ml Teflon-sealed autoclave and heated at 120 ºC for 24 h. After cooling down to room temperature, the CNTs/Co_3O_4 intermediate was collected by centrifugation and washed with ethanol.

2.3 Conversion of CNTs/Co_3O_4 intermediate to CNTs/Co@C hybrid

The CNTs/Co@C hybrid was produced by mixing the as-prepared CNTs/Co_3O_4 intermediate (0.6 g) with pyrrole (0.5 ml) in a stainless steel autoclave, and then the tightly sealed autoclave was heated at 550 ºC for 6 h in a furnace. The Co@C nanoparticles were synthesized using a similar method as above without the addition of CNTs.

2.4 Characterizations

The morphology was examined by transmission electron microscope (TEM: JEOL JEM-2100) at an accelerating voltage of 200 kV. The phase structures of all samples were determined from 10° to 90° on a powder X-ray diffraction (XRD) using Cu Kα radiation (λ = 0.154 nm). Raman spectroscopy was carried out on a Renishaw

inVia Raman microscope with an excitation wave length of 633 nm. Thermogravimetry curves (TG) of the samples were recorded on an SDT Q600 TGA analyzer under air in the temperature range of 30-800 ºC with a heating rate of 5 ºC min^{-1}. The magnetic properties of the as-prepared CNTs/Co@C hybrid were measured by a Lake Shore 7404 vibration sample magnetometer (VSM) at room temperature.

2.5 Electromagnetic Wave Absorption Property Measurements

For the fabrication of samples used for EM wave absorption test, the as-prepared CNTs/Co@C powders were dispersed in epoxy resin homogeneously (mass ratio of 60% and 40%), and then pressing it into cylindrical specimens with an inner diameter of 3.04 mm, outer diameter of 7.00 mm, and thickness of 2.00 mm according to the procedure described in our previous work.[15] The scattering parameters were obtained by using an Agilent Technologies E8363A vector network analyzer in 1.0-20.0 GHz. Afterward, the complex permittivity (ε_r) and permeability (μ_r) of the samples were determined from the measured scattering parameters. Finally, the RL values can be calculated from the relative permittivity and permeability at the given frequency and absorber thickness by using the following formulas:[39, 40]

$$Z_{in} = Z_0(\mu_r/\varepsilon_r)^{1/2} \tanh\{ j(2\pi fd/c)(\mu_r\varepsilon_r)^{1/2}\} \quad (1)$$

$$RL = 20\log\left|(Z_{in} - Z_0)/(Z_{in} + Z_0)\right| \quad (2)$$

where Z_0 refers to the input impedance of free space, Z_{in} is the input impedance of the absorber, f is the frequency, c is the velocity of light, and d is the absorber thickness. The EM performances of the direct mixture of CNTs and Co@C beads in epoxy resin were carried on using the above procedures. The weight ration of CNTs, Co@C beads

and epoxy resin is 25%: 25%: 50%.

3. Results and discussion

3.1 Phase, morphology and microstructure analysis

The XRD patterns of the as-synthesized CNTs/Co@C hybrid, CNTs/Co_3O_4 intermediate and pure CNTs are presented in Fig. 1a. For pure CNTs, a broad diffraction peak centered at $2\theta = 22°$ can be observed, confirming the existence of amorphous carbon in CNTs. The intensive peak at 26° refers to (002) plane of the stacked graphene layers of CNTs.[41] After the solvothermal process, apart from a weak characteristic peak ($2\theta = 22°$) of CNTs, all the other diffraction peaks can be well indexed to a cubic phase of Co_3O_4 (JCPDS Card No. 42-1467), suggesting a successful formation of CNTs/Co_3O_4 composites. After the carbon reduction process, the diffraction peaks at 44°, 51° and 75° are precisely in agreement with (200), (111) and (220) planes of face-centered cubic Co (JCPDS Card No. 15-0806), while the CNTs related peak remained unchanged and no additional peaks are detected, indicating the complete reduction of Co_3O_4 to Co. Fig. 1b shows the Raman spectra of pure CNTs and CNTs/Co@C hybrid. As can be seen, all samples display two distinguishable peaks centered at about 1331 cm^{-1} and 1573 cm^{-1}, respectively, which correspond to the D-band from amorphous carbon and G-band from graphite carbon. [42]The intensity ratio of D band and G band (I_D/I_G) is usually employed to evaluate the order degree of carbon atoms. Compared with pure CNTs (1.31), the I_D/I_G value for CNTs/Co@C hybrid (1.43) is larger, implying that the CNTs/Co@C hybrid owns an increased disorder degree of carbon, mainly attributing to the amorphous carbon

residue coated on Co beads during the reduction.

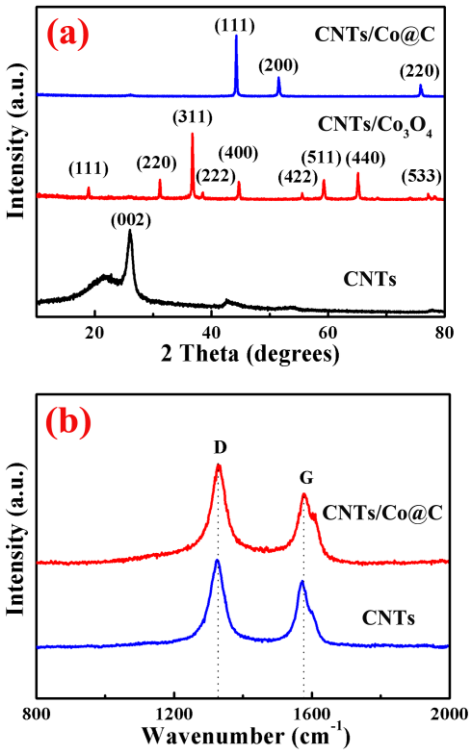

Fig. 1 (a) XRD spectra of CNTs/Co@C hybrid, CNTs/Co_3O_4 intermediate, and pure CNTs. (b) Raman spectra of CNTs/Co@C hybrid and pure CNTs.

The morphology and microstructure of the samples were revealed by SEM, TEM and HR-TEM observation. As shown in Fig. 2a and b, the as-obtained CNTs/Co_3O_4 intermediate presented a composite structure, in which Co_3O_4 spheres with sizes of 200-300 nm were threaded by carbon nanotubes. From the magnified HR-TEM image, two types of lattice fringe distances of 0.338 nm and 0.454 nm correspond to the (002) plane of CNTs and (111) plane of Co_3O_4, respectively. Fig. 2c-f display TEM and HR-TEM images of the CNTs/Co@C hybrid with different magnifications. After the carbon reducing treatment on CNTs/Co_3O_4, as presented in Fig. 2c, no obvious variation was detected in over-all morphology. Fig. 2d shows a representative image of an individual Co bead, and it is found that carbon nanotube passes through Co bead,

which is composed of numerous small particles. From the enlarged image (Fig. 2e, f), it is visible that a carbon layer (ca. 5 nm) is coated on the surface of Co beads, resulting in a core-shell structure and the lattice fringe distance of 0.221 nm can match well with the (111) plane of face-centered Co in accordance with the XRD characterization, further confirming the formation of CNTs/Co@C hybrid.

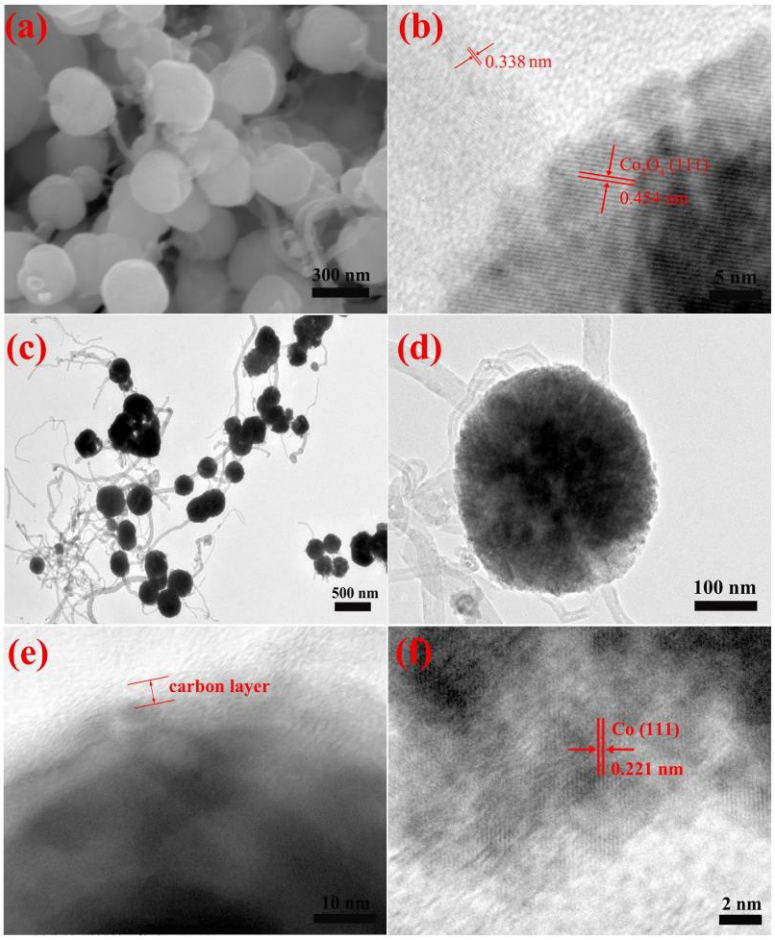

Fig. 2 SEM, TEM and HR-TEM images of CNTs/Co_3O_4 intermediate (a, b) and CNTs/Co@C hybrid (c-f) with different magnifications.

On the basis of the above experimental results, a possible formation process of CNTs/Co@C hybrid was accordingly proposed (Fig. 3). Firstly, after the acid treatment, the CNTs surface was negatively charged and possess lots of functional groups (-COOH, -OH, *etc*). Co^{2+} ions were randomly attracted onto the sidewalls of

CNTs to form nucleation sites. During the reaction, the residual cobalt ions were continuously adsorbed on the nucleation sites and slowly crystallized to form Co_3O_4 beads. With further carbon reduction process, pyrrole was firstly evaporated and diffused on the surface of Co_3O_4 beads and CNTs with increasing temperature. When the temperature was increased to 550 ºC, carbon was generated due to the pyrolysis of pyrrole causing the reduction of cobalt oxide to cobalt, and the residual carbon was formed a coated layer on the surface of Co beads simultaneously.

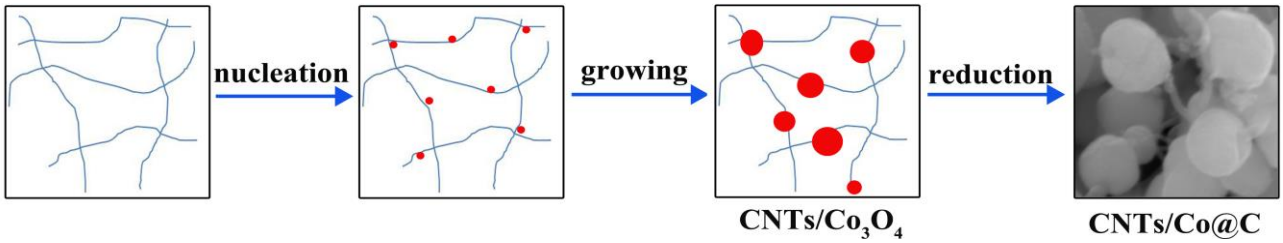

Fig. 3 Schematic illustration for the preparation of CNTs/Co@C hybrid.

To quantify the weight ratio of carbon in the CNTs/Co@C hybrid, TGA analysis was carried out in air at a heating rate of 5 ºC min^{-1}. As shown in Fig. 4, the weight loss process can be divided into three stages. Firstly, a slight weight loss of ca. 2.0% observed below 150 ºC is ascribed to the evaporation of water absorbed on the surface of the sample. From 150 to 350 ºC, an intense weight increase of 7.1% occurred indicating the oxidation of Co to Co_3O_4. In the third stage, the weight loss of 8.3% is associated with the oxidation of carbon to form CO and CO_2 in the temperature range of 350-600 ºC. After 600 ºC, no obvious weight loss was observed, indicating the complete oxidation of carbon and only Co_3O_4 was left. Hence, the total 96.8% weight (100%-2.0%+7.1%-8.3%) refers to the left Co_3O_4. Based on the above analysis, the content of carbon in the CNTs/Co@C hybrid can be calculated by the following

equation:

$$wt\%_L = \frac{(1 - wt\%_{carbon} - wt\%_{water})}{3M_{Co}} \times M_{Co_3O_4} \quad (3)$$

where $wt\%_L$ is the weight percentage of left Co_3O_4, and M represents molecular weight of the chemicals. The weight ratio of carbon in the CNTs/Co@C hybrid was calculated to be ca. 29.8 wt%, and Co content is about 70.2 wt%.

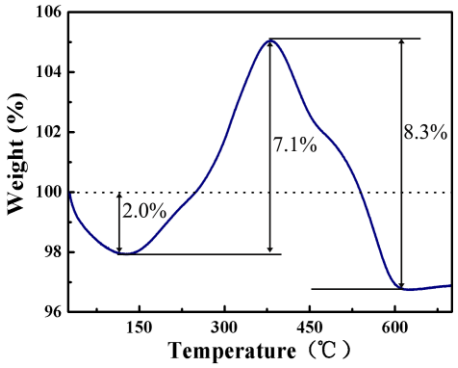

Fig. 4 TGA curve of CNTs/Co@C hybrid heated in air.

3.2 Magnetic property of CNTs/Co@C hybrid

The magnetic property of the CNTs/Co@C hybrid was investigated at room temperature. From the magnetic hysteresis loop (Fig. 5), the saturation magnetization (M_s) value for the CNTs/Co@C hybrid is ca. 82.5 emu g^{-1}, which is obviously lower than that of bulk Co (162.5 emu g^{-1}).[14] The decrease of M_s is mainly ascribed to the presence of non-magnetic carbon. Besides, the Co beads composed of nanoparticles have induced an enhancement of spin disorder, also probably leading to a decrease in saturation magnetization of CNTs/Co@C hybrid. However, the CNTs/Co@C hybrid shows a larger H_c value of 258.8 Oe comparing with bulk Co (ca. 10 Oe).[14] It has been widely investigated that H_c value is strongly related to the morphology, shape, and particle size of samples. According to the TEM images (Fig. 2), the Co beads were

assembled by numerous Co nanoparticles, which induced high surface anisotropy, giving rise to an enhancement of coercivity.

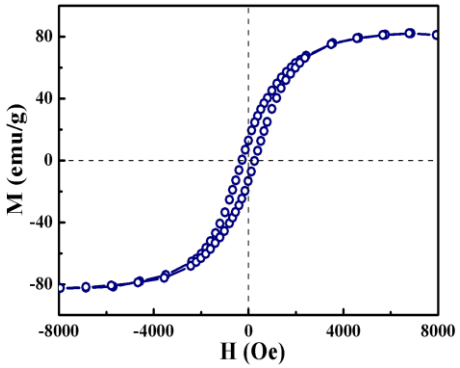

Fig. 5 Magnetic hysteresis loop of CNTs/Co@C hybrid measured at room temperature.

3.3 EM absorption performances

The EM absorption performances of materials are strongly associated with their relative permittivity ($\varepsilon_r = \varepsilon_r' - j\varepsilon_r''$) and permeability ($\mu_r = \mu_r' - j\mu_r''$). Figs. 6a-d exhibit the frequency-dependent complex permittivity and permeability for the epoxy resin composites containing 60 wt% and 40 wt% CNTs/Co@C hybrid over 1-20 GHz range. As shown in Figs. 6a and b, the real part of permitivity (ε_r') manifests a similar variation for two samples, in which the ε_r' values all tend to decrease continuously versus increasing frequency. The value of ε_r' is lessened from 32.2 to 17.9 for the sample with 60 wt% loading, while it reduced from 18.8 to 11.5 for the CNTs/Co@C-epoxy resin composites with 40 wt% filler content. With regard to the imaginary part of the permittivity (ε_r'') for two samples, the ε_r'' curves all exhibit a peak at ca. 17.5 GHz. For the epoxy resin composite with 60 wt% filler, one weak peak at about 8.9 GHz and two strong peaks at 13.6 and 17.2 GHz can be observed,

implying a dielectric resonance behavior. The appearance of multiple resonance peaks can be explained by the following aspects. Firstly, the defects existed in the coated amorphous carbon have caused dipole polarizations at microwave absorption frequency. Secondly, two kinds of interfaces including amorphous carbon layer-Co and Co-CNTs interfaces are present, thus producing multiple interface polarizations (called as Maxwell-Wagner effect) due to the charges accumulation at the heterointerfaces.[43] Notably, as compared to the sample with 60 wt% loading, the 40 wt% CNTs/Co@C-epoxy resin composites show a lower permittivity level, which can be mainly ascribed to the increase of space charge polarization among Co particles being isolated more effectively by epoxy resin.

Fig. 6c indicates that the μ_r' curve for the sample with 60 wt% loading fluctuates from 1.39 to 0.91 over the 1.0-18.4 GHz range, and then increases to 1.13 as increasing frequency to 20 GHz. While for the imaginary part μ_r'', a broad resonance peak is observed in the 1-17.2 GHz with a maximum point of 0.17 at ca. 7.6 GHz. Conventionally, the magnetic loss of magnetic materials mainly derives from hysteresis loss, domain-wall resonance, natural resonance, and eddy current loss.[34,44] The magnetic hysteresis loss stemming from the irreversible magnetization is only generated in a strong magnetic field. The domain wall resonance can be neglected in this work because it usually occurs at a low frequency range (MHz). Hence, the natural resonance or eddy current loss should be responsible for the magnetic loss. The natural resonance frequency can be evaluated by the following equations:[45]

$$K = \mu_0 M_S H_C / 2 \quad (4)$$

$$H_a = 4|K|/3\mu_0 M_S \quad (5)$$

$$2\pi f_r = \gamma H_a \quad (6)$$

where γ represents the gyromagnetic ratio, μ_0 is the permeability constant in free space, K is the magnetocrystalline anisotropy constant, H_a is the anisotropy field and f_r is the nature resonance frequency. It can be concluded from the above equations that the nature resonance frequency is proportional to the anisotropy field (H_a), which also affects the H_c value in proportion. As presented in Fig. 5, compared to bulk cobalt (ca. 10 Oe), the CNTs/Co@C hybrid exhibited a larger H_c value (258.8 Oe), and thus the natural resonance frequency was located at high GHz range. As for most soft magnetic materials, their H_a and H_c values are quite low, leading to a low f_r value. According to the quarter-wavelength model ($t_m = nc/4 f_m(\varepsilon_r \mu_r)^{1/2}$), the H_c value for the CNTs/Co@C hybrid is 258.8 Oe, which is much larger than the reported $Fe_{50}Co_{50}$ alloy (135 Oe),[46] RGo-Fe_3O_4 nanocomposites (53.6 Oe),[47] and $Co_{20}Ni_{80}$ alloy (<100 Oe),[48] in favor of achieving thin absorption thickness at high frequency. Eddy current loss is another factor that can influence the magnetic loss, and can be calculated by equation (7):[49]

$$\mu_r''(\mu_r')^{-2} f^{-1} = 2\pi\mu_0 d^2\sigma \quad (7)$$

where σ and d represent the electric conductivity and thickness of the composite, μ_0 is the permeability of vacuum. If the magnetic loss mainly originates from eddy current loss, then values of $\mu_r''(\mu_r')^{-2} f^{-1}$ should be constant with the variation of frequency. However, it can be found from Fig. 7 that, the values for both samples show obvious fluctuations, suggesting that the eddy current loss is not main effect factor on the

magnetic loss, and thus the magnetic loss of the CNTs/Co@C hybrid is mainly resulted from the natural resonance. For another sample with 40 wt% loading content, the μ_r'' curve also exhibits a weak and broad resonance peak in the 1-17.5 GHz with a maximal value of 0.11 at ca. 10 GHz (Fig. 6d). The maximum μ_r'' value is lower than that of the sample with 60 wt% CNTs/Co@C (0.17), due to the decreased addition amount of CNTs/Co@C. Notably, the μ_r'' values are less than zero in the 8.9-20 GHz range, denoting that the Co/CNTs nanocomposites could be used as a left-hand material. Notably, the μ_r'' values are less than zero in the 8.9-20 GHz range, denoting that the Co/CNTs nanocomposites could be used as a left-hand material.[50-52] For a further investigation, the dielectric loss tangent ($\tan\delta_E = \varepsilon''/\varepsilon'$) and magnetic loss tangent ($\tan\delta_M = \mu''/\mu'$) were calculated for two samples and displayed in Figs. 6e and f. All samples show a similar tendency that the dielectric loss increases and magnetic loss decreases with the increasing frequency. For the sample with 60 wt% loading, the $\tan\delta_E$ and $\tan\delta_M$ values show little difference in the frequency range of 1-7.5 GHz (Fig. 6e), demonstrating that the dielectric and magnetic losses both exist in this frequency region. From 7.5 to 20 GHz, the strong dielectric loss and relatively weak magnetic loss are observed, suggesting that the dielectric loss has significant effect on EM absorption, especially at high frequency. When the CNTs/Co@C content is reduced to 40 wt%, the $\tan\delta_E$ and $\tan\delta_M$ values (Fig. 6f) are lower than those of the sample with 60 wt% loading. Interestingly, it can be observed that $\tan\delta_E$ and $\tan\delta_M$ curves show the inversed variation trend for both samples. The reason can be explained through the transformation between magnetic energy and electric energy. It

is widely known the positive μ_r'' and ε_r'' represent the storage capacity of magnetic energy and electric energy. Contrarily, a negative μ_r'' value at high frequency suggests that the magnetic energy is released from the samples. Based on the Maxwell equations, a magnetic field can be induced by an alternating electric field derived from the movement of charges. The radiated out magnetic energy transferred to electric energy, which enhanced ε_r'' and caused the decrease of μ_r'', giving rise to the reversed change trend of $\tan\delta_E$ and $\tan\delta_M$. Fig. 6c and d showed that the imaginary part (μ_r'') decreased gradually with frequency to negative between 15-20 GHz, illustrating that the magnetic energy was induced and released from the Co/CNTs@C hybrid in high frequency region. The transformation of magnetic energy to electric energy indicates that, at high frequency, the EM absorption is mainly ascribed to the dielectric loss in the CNTs/Co@C hybrid. The negative permeability value and totally contrary variation trend of tangent loss have also been observed in other magnetic carbon hybrids such as CNTs/wax composite,[52] Fe/Co/Ni nanoparticles coated carbon nanofibers,[53] graphene oxide/CNT-Fe_3O_4 composite,[32] and porous carbon/Co hybrid.[54]

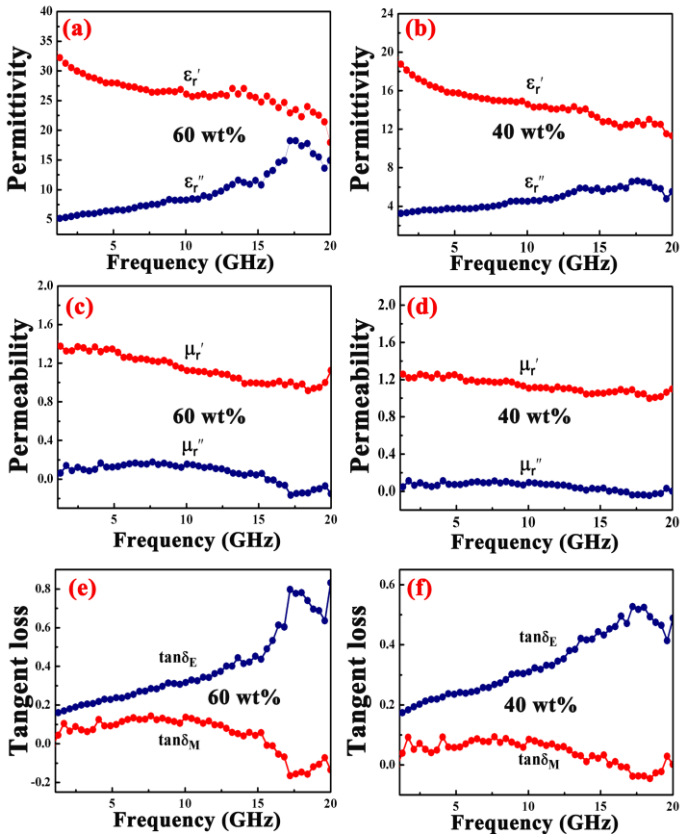

Fig. 6 Frequency dependence of complex permittivity (a, b), complex permeability (c, d), dielectric and magnetic loss tangent (e, f) for the epoxy resin composites with different CNTs/Co@C loadings.

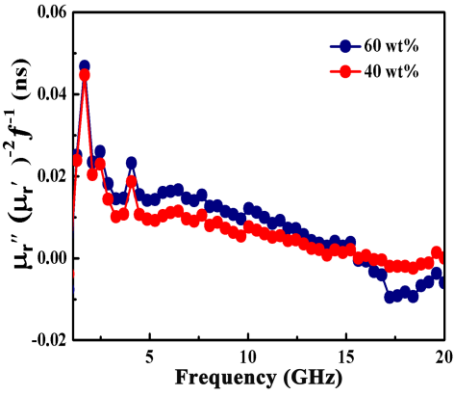

Fig. 7 $\mu_r''(\mu_r')^{-2} f^{-1}$ values of CNTs/Co@C hybrid as a function of frequency.

To reveal the EM wave absorption performances of the the CNTs/Co@C hybrid, the RL values were calculated according to equation (1) and (2). In general, when evaluating the EM absorption performances of absorbers, three factors should be

considered: the minimal RL peak, the effective bandwidth (RL<-10 dB, corresponding to 90% microwave absorption), and the absorber thickness. Fig. 8 displays the calculated RL curves versus frequency for the CNTs/Co@C-epoxy resin composites with different loadings at various thicknesses over the 1-20 GHz range. For the CNTs/Co@C-epoxy resin composites with 60 wt% loading (Fig. 8a), a minimal RL value of -23.2 dB is obtained at 4.9 GHz with a matching thickness of 2.5 mm. The RL values exceeding -10 dB were observed in a wide frequency range of 1.5-15 GHz as the absorber thickness ranges from 1.0 to 7.5 mm, showing superior EM absorption in S-band (2-4 GHz). In the lower loading concentration of 40 wt%, as displayed in Fig. 8b, the optimal reflection loss is -31.5 dB at 9.3 GHz and the bandwidth of RL below -10 dB is 3.2 GHz (8.1-11.3) with a thin thickness of 2 mm. The effective absorption (below -10 dB) can be adjusted between 1.6 and 20.0 GHz for the absorber with thickness ranging from 1.0 to 10.0 mm. These results indicate that the CNTs/Co@C hybrid possesses remarkable absorption from C to K_u band. Compared to the composites containing 60 wt% CNTs/Co@C hybrid, the sample with lower concentration (40 wt%) possesses a stronger absorption intensity and wider effective absorption frequency range. However, the composites with 60 wt% CNTs/Co@C hybrid show thinner absorption thicknesses (*e.g.*, 4 mm at 2.5 GHz) than the sample with 40 wt% (6 mm at 2.5 GHz) at the same frequencies. Besides, it can be seen from Fig. 8 that both of the samples present a similar tendency that the optimal RL peaks are tuned to low frequency range. Such a shift can be well explained by the quarter-wavelength matching model ($t_m=nc/4f_m(\varepsilon_r\mu_r)^{1/2}$), in which the

thickness is inversely proportional to frequency. For more comparisons, the EM absorption performances of the CNTs/Co@C hybrid and some earlier reported absorbents including Co nanomaterials, pure CNTs, and magnetic carbon hybrids are summarized in Table 1. As can be seen, in comparison with the previously reported Co flowers,[55] Co particles[56] and pure CNTs,[57] the as-synthesized CNTs/Co@C hybrids exhibit stronger absorption capacity and broader absorption bandwidth, which is mainly ascribed to the effective combination of magnetic loss from Co nanospheres and the dielectric loss from CNTs. Comparing with some magnetic CNTs nanocomposites, the CNTs/Co@C hybrid display stronger microwave absorption intensity. For example, the CNTs/Ni nanocomposites,[35] Fe filled CNTs nanocomposites,[57] and CNTs/Fe_3O_4 nanopowders[58] showed a minimum RL value of -11.9 dB, -18.2 dB and -24.8 dB respectively, which is larger than that of the CNTs/Co@C hybrid (-31.5 dB). Moreover, when locating at the same frequency under effective microwave absorption (RL< -10 dB), the samples with 60 wt% CNTs/Co@C show thinner thickness (*e.g.*, 3 mm at ca. 4 GHz) as compared to that of GO/CNT-Fe_3O_4 (*e.g.*, 5 mm at 4 GHz).

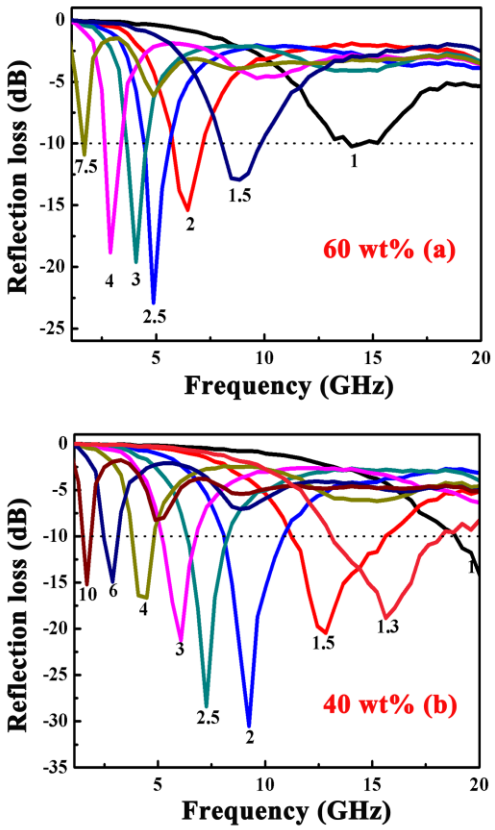

Fig. 8 Reflection loss curves of 60 wt% (a) and 40 wt% (b) CNTs/Co@C-epoxy resin composites at various thicknesses in the frequency range of 1-20 GHz.

Table 1 Comparisons of some earlier reported Co and magnetic CNTs hybrids.

Sample	Mass ratio (wt%)	Minimum RL (dB)	dm (minimal RL)	dm (RL < -10 dB)	Frequency range (GHz) (RL < -10 dB)	Ref.
Co flower	60	-11.6	2	----	----	55
Co particles	70	-19.1	5	3.0-5.5	8.1-18	56
pure CNTs	20	-11.2	3.5	----	13.2-13.5	57
CNTs/Ni	50	-11.9	4	3.0-4.0	3-4	35
CNTs/Fe_3O_4	70	-18.2	----	----	10.5-12.4	58
Fe filled CNTs	20	-22.7	3.5	----	13.2-17.4	57
GO/CNT-Fe_3O_4	30	-31.3	5	2.0-5.0	2-18	10
CNTs/Co@C	60	-23.2	2.5	1.0-7.5	1.5-15	this work
CNTs/Co@C	40	-31.5	2.0	1.0-10.0	1.6-20	this work

For illustrating the effects of Co@C nanoparticles on CNTs more clearly, the EM absorption performances of a directly mixture of CNTs and Co@C nanoparticles in

epoxy resin were also carried, which is shown in Fig. 9a and b. It is observed that the samples present much higher values of ε_r' and ε_r'' than the CNTs/Co@C-epoxy resin composites, while the permeability values show a similar tendency with 40 wt% CNTs/Co@C-epoxy resin composites. Fig. 9b displays the calculated RL curves of the directly mixture of CNTs and Co@C nanoparticles in epoxy resin with different thicknesses over 1-20 GHz. Clearly, this directly mixture displays rather poor EM absorption with the minimal RL value is only -11.4 dB and there is no bandwidth under -10 dB. This phenomenon again verifies the importance of matched characteristic impedance and also suggests Co@C beads deposited on the CNTs surface can improve the impedance matching of CNTs/Co@C hybrid effectively by decreasing the complex permittivity and increasing the permeability.

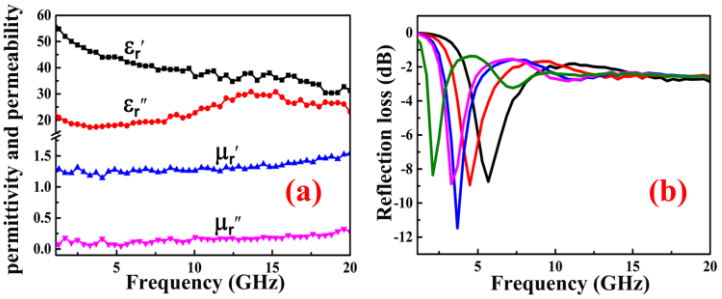

Fig. 9 (a) Complex permittivity and permeability, (b) Reflection loss curves of a direct mixture of CNTs and Co@C beads in epoxy resin in the frequency range of 1-20 GHz.

In order to investigate the possible mechanism for the enhanced EM absorption performances, the quarter-wavelength matching model was employed, in which the minimal RL can be achieved at a certain frequency if the absorber thickness complies with the following equation:[27]

$$t_m = nc/4 f_m(\varepsilon_r \mu_r)^{1/2} \quad (8)$$

where f_m is the peak frequency of RL, t_m is the absorber thickness, λ is the wavelength of EM wave, μ_r and ε_r are the measured complex permeability and permittivity values at f_m, and c is the velocity of light in vacuum. When an EM wave is incident on the absorber supported by a metal plate, it is partially reflected from the air-absorber interface and from the absorber-metal interface. According to the quarter-wavelength matching model, if the absorber thickness at a certain frequency satisfies equation (8), these two reflected EM waves are out of phase by 180° and cancel out each other at the air-absorber interface. Fig. 10a shows the RL curves versus frequency for the 40 wt% CNTs/Co@C-epoxy resin composites under different thicknesses. On the basis of quarter wavelength equation (λ/4), a simulated curve between the matching thickness (t_m) and peak frequency (f_m) for the composites is displayed in Fig. 10b. The red circles represent the matching thickness at the peak frequency, which are directly obtained from the RL curves in Fig. 10a. Obviously, all the red circles are located around the t_m=λ/4 curve, suggesting that the relationship between the experimental matching thickness (t^{exp}_m) and peak frequency for the CNTs/Co@C hybrid obeyed the quarter wavelength cancellation condition. Fig. 10c presents the frequency dependence of $Z=|Z_{in}/Z_0|$ (blue solid curve), in which the frequency dependence of RL values under a thickness of 2 mm is also shown (red dashed curve). The optimal RL value can be achieved at 9.3 GHz, while the corresponding Z value is close to 1.0 and the matching thickness of 2 mm is on the λ/4 curve (Fig. 10b). These results indicate that the minimal RL value can be obtained when the relationship

between the matching thickness and frequency for the CNTs/Co@C hybrid complies well with the quarter wavelength model. It also suggests that the quarter wavelength theory can serve as an ideal guide for designing the required thicknesses for EM absorption, once the corresponding complex permeability and permittivity are measured.

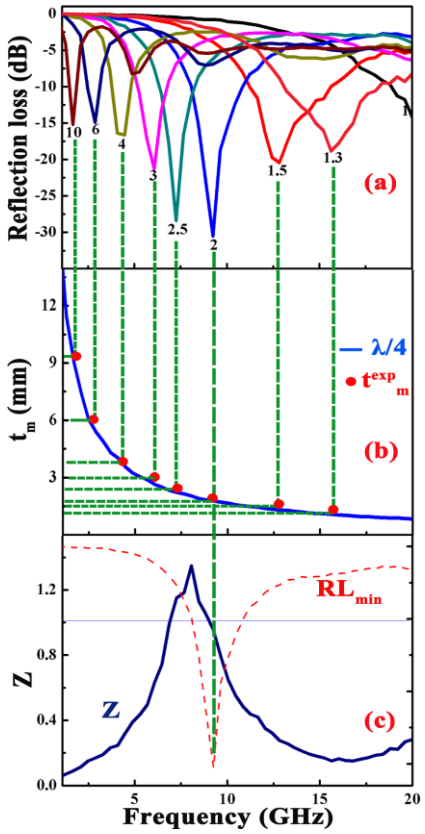

Fig. 10 (a) Frequency dependence of RL values for CNTs/Co@C hybrid (40 wt%) with various thicknesses; (b) simulated curves of the absorber thicknesses (t_m) against peak frequency (f_m); (c) the values of normalized input impedance ($|Z_{in}/Z_0|$) for CNTs/Co@C hybrid (40 wt%).

Conclusions

In conclusion, the CNTs/Co@C hybrid has been synthesized successfully through a feasible solvothermal way followed by a carbon reduction process. Combining the

magnetic loss of Co beads with dielectric loss from CNTs as well as a better impedance matching, the CNTs/Co@C hybrid exhibits improved EM absorption properties in contrast with previously reported Co nanomaterials and pure CNTs or some other magnetic CNTs composites. This research suggests an efficient way to synthesize high-efficiency EM wave absorption materials with light weight, strong absorption, wide absorption frequency range, and thin thickness.

Acknowledgements

The authors acknowledge the financial support from the National Natural Science Foundation of China (No. 51572157), the Fundamental Research Funds of Shandong University (2015JC016, 2015JC036), the Science and Technology Development Plan (2014GGX102004).

References:

1 F. Wang, J. Liu, J. Kong, Z. Zhang, X. Wang, M. Itoh and K. Machida, *Journal of Materials Chemistry*, 2011, 21, 4314-4320.

2 M. Lu, W. Cao, H. Shi, X. Fang, J. Yang, Z. Hou, H. Jin, W. Wang, J. Yuan and M. Cao, *Journal of Materials Chemistry A*, 2014, 2, 10540-10547.

3 C. Liang, C. Liu, H. Wang, L. Wu, Z. Jiang, Y. Xu, B. Shen and Z. Wang, *Journal of Materials Chemistry A*, 2014, 2, 16397-16402.

4 B. Zhao, W. Zhao, G. Shao, B. Fan, and R. Zhang, *ACS Applied Materials &Interfaces*, 2015, 7, 12951-12960.

5 X. Liu, Y. Chen, X. Cui, M. Zeng, R. Yu and G. Wang, *Journal of Materials Chemistry A*, 2015, 3, 12197-12204.

6 J. Liu, M. Cao, Q. Luo, H. Shi, W. Wang and J. Yuan, *ACS Applied Materials &Interfaces*, 2016, 8, 22615-22622.

7 R. Qiang, Y. Du, H. Zhao, Y. Wang, C. Tian, Z. Li, X. Han and P. Xu, *Journal of Materials Chemistry A*, 2015, 3, 13426-13434.

8 Y. Lü, Y. Wang, H. Li, Y. Lin, Z. Jiang, Z. Xie, Q. Kuang and L. Zheng, *ACS Applied Materials&Interfaces*, 2015, 7, 13604-13611.

9 J. Feng, F. Pu, Z. Li, X. Li, X. Hu and J. Bai, *Carbon*, 2016, 104, 214-225.

10 L. Wang, X. Jia, Y. Li, F. Yang, L. Zhang, L. Liu, X. Ren and H. Yang, *Journal of Materials Chemistry A*, 2014, 2, 14940-14946.

11 C. Tsonos, N. Soin, G. Tomara, B. Yang, G. C. Psarras, A. Kanapitsas and E. Siores, *RSC Advances*, 2016, 6, 1919-1924.

12 G. Pan, J. Zhu, S. Ma, G. Sun and X. Yang, *ACS Applied Materials&Interfaces*, 2013, 5, 12716-12724.

13 J. Shen, Y. Yao, Y. Liu and J. Leng, *Journal of Materials Chemistry C*, 2016, 4, 7614-7621.

14 C. He, S. Qiu, X. Wang, J. Liu, L. Luan, W. Liu, M. Itoh and K. Machida, *Journal of Materials Chemistry*, 2012, 22, 22160-22166.

15 C. Wang, X. Han, X. Zhang, S. Hu, T. Zhang, J. Wang, Y. Du, X. Wang and P. Xu, *Journal of Physical Chemistry C*, 2010, 114, 14826–14830.

16 B. Zhao, X. Guo, W. Zhao, J. Deng, G. Shao, B. Fan, Z. Bai and R. Zhang, *ACS Applied Materials&Interfaces*, 2016, 8, 28917-28925.

17 B. Zhao, G. Shao, B. Fan, W. Zhao, R. Zhang, *Physical Chemistry Chemical. Physics*, 2015, 17, 2531-2539.

18 C. Liang, C. Liu, H. Wang, L. Wu, Z. Jiang, Y. Xu, B. Shen and Z. Wang, *Journal of Materials Chemistry A*, 2014, 2, 16397-16402.

19 Z. Wang, L. Wu, J. Zhou, Z. Jiang and B. Shen, *Journal of Materials Chemistry A*, 2014, 6, 12298-12302.

20 P. Liu, Y. Huang, J. Yan, Y. Yang and Y. Zhao, *ACS Applied Materials&Interfaces*, 2016, 8, 5536-5546.

21 M. Han, X. Yin, L. Kong, M. Li, W. Duan, L. Zhang and L. Cheng, *Journal of Materials Chemistry A*, 2014, 2, 16403-16409.

22 X. Zhang, G. Ji, W. Liu, X. Zhang, Q. Gao, Y. Li and Y. Du, *Journal of Materials Chemistry C*, 2016, 4, 1860-1870.

23 N. Li, M. Cao and C. Hu, *Journal of Materials Chemistry*, 2012, 22, 18426-18432.

24 J. Zhu, S. Wei, N. Haldolaarachchige, D. Young and Z. Guo, *Journal of Physical Chemistry C*, 2011, 115, 15304-15301.

25 C. Feng, X. Liu, Y. Sun, C. Jin and Y. Lv, *RSC Advances*, 2014, 4, 22170-22175.

26 H. Wang, L. Wu, J. Jiao, J. Zhou, Y. Xu, H. Zhang, Z. Jiang, B. Shen and Z. Wang, *Journal of Materials Chemistry A*, 2015, 3, 6517-6525.

27 X. Li, J. Feng, Y. Du, J. Bai, H. Fan, H. Zhang, Y. Peng and F. Li, *J. Mater. Chem. A*, 2015, 3, 5535-5546.

28 Y. Chen, G. Xiao, T. Wang, Q. Ouyang, L. Qi, Y. Ma, P. Gao, C. Zhu, M. Cao and H. Jin, *Journal of Physical Chemistry C*, 2011, 115, 13603-13608.

29 D. Micheli, A. Vircella, R. Pastore and M. Marchetli, *Carbon*, 2014, 77, 130-142.

30 W. Song, M. Cao, L. Fan, M. Lu, Y. Li, C. Wang and H. Ju, *Carbon*, 2014, 77, 130-142.

31 Y. Zhan, R. Zhao, Y. Lei, F. Meng, J. Zhong and X. Liu, *Journal of Magnetism and Magnetic Materials*, 2011, 323, 1006-1010.

32 L. Wang, X. Jia, Y. Li, F. Yang, L. Zhang, L. Liu, X. Ren and H. Yang, *J. Mater. Chem. A*, 2014, 2, 14940-14946.

33 S. Zhang, Q. Zhang, Y. Zhao, Q. Jiao, X. Ni, Y. Wang, Y, Cheng and C. Ding, *Journal of Alloys and Compounds*, 2017, 694, 309-312.

34 F. Wen, F. Zhang and Z. Liu, *Journal of Physical Chemistry C*, 2011, 115, 14025-14030.

35 H. Zhao, X. Han, M. Han, L. Zhang and P. Xu, *Materials Science Engineering B*,

2010, 167, 1-5.
36 B. P. Singh, D. K. Saket, A. P. Singh, S. Pati, T. K. Gupta, V. N. Singh, S. R. Dhakate, S. K. Dhawan, R. K. Kotnala and R. B. Mathur, *Journal of Materials Chemistry A*, 2015, 3, 13203-13209.
37 C. Bittencourt, A. Felten, J. Ghijsen, J. J. Pireaux, W. Drube, R. Erni and G. Van Tendeloo, *Chemical Physics Letter*, 2007, 436, 368-372.
38 T. Bao, Y. Zhao, X. Su and Y. Duan, *Materials Science Engineering B*, 2011, 176, 906-912.
39 J. Liu, M. Itoh and K. Machida, *Applied Physics Letters*, 2003, 83,4017-4019.
40 H. Wang, L. Wu, J. Jiao, J. Zhou, Y. Xu, H. Zhang, Z. Jiang, B. Shen and Z. Wang, *Journal of Materials Chemistry A*, 2015, 3, 6517-6525.
41 X. Li, H. Gu, J. Liu, H. Wei, S. Qiu, Y. Fu, H. Lv, G. Lu, Y. Wang and Z. Guo, *RSC Advances*, 2015, 5, 7237-7244.
42 M. Lu, M. Cao, Y. Chen, W. Cao, J. Liu, H. Shi, D. Zhang, W. Wang and J. Yuan, *ACS Applied Materials&Interfaces*, 2015, 7, 19408-19415.
43 B. D. Bertram and R. A. Gerhardt, *Journal of American Ceramic Society*, 2011, 94, 1125-1132.
44 Y. Du, W. Liu, R. Qiang, Y. Wang, X. Han, J. Ma and P. Xu, *ACS Applied Materials&Interfaces*, 2014, 6, 12997−13006.
45 C. Kittel, *Physics Review*, 1948, 73, 155-161.
46 H. Lv, G. Ji, M. Wang, C. Shang, H. Zhang, and Y. Du, *Journal of Alloys and Compounds*, 2014, 615, 1037-1042.
47 X. Sun, J. He, G. Li, J. Tang, T. Wang, Y. Guo and H. Xue, *Journal of Materials Chemistry C*, 2013, 1, 765-777.
48 M. Yasir Rafique, L. Panb and A. Farid, *Journal of Alloys and Compounds*, 2016,

656, 443-451.

49 M. Wu, Y. Zhang, S. Hui, T. Xiao, S. Ge, W. Hines, J. Budnick and G. Taylor, *Applied Physics Letters*, 2002, 80, 4404-4406.

50 D. Smith, W. Padilla, D. Vier, S. Nemat-Nasser and S. Schultz, *Physics Review Letters*, 2000, 84, 4184-4187.

51 T. Kasagi, T. Tsutaoka and K. Hatakeyama, *Applied Physics Letters*, 2006, 88, 172502.

52 L. Deng and M. Han, *Applied Physics Letters*, 2007, 91, 023119.

53 J. Xiang, J. Li, X. Zhang, Q. Ye, J. Xu and X. Shen, *Journal of Materials Chemistry C*, 2014, 2, 16905-16914.

54 Q. Liu, D. Zhang and T. Han, *Applied Physics Letters*, 2008, 93, 013110.

55 C. Wang, X. Han, X. Zhang, S. Hu, T. Zhang, J. Wang, Y. Du, X. Wang and P. Xu, *Journal of Physical Chemistry C*, 2010, 114, 14826-14830.

56 S. Wen, Y. Liu, X. Zhao, J. Cheng and H. Li, *Powder Technology*, 2014, 264, 128-132.

57 H. Li, H. Zhu, H. Guo and L. Yu, *Materials Letters*, 2007, 61, 3547-3550.

58 H. Cui, T. Li, T. Zhao, H. Liu, L. Liu, and W. Zhang, New Carbon Materials, 2013, 28, 184-190.

TOC

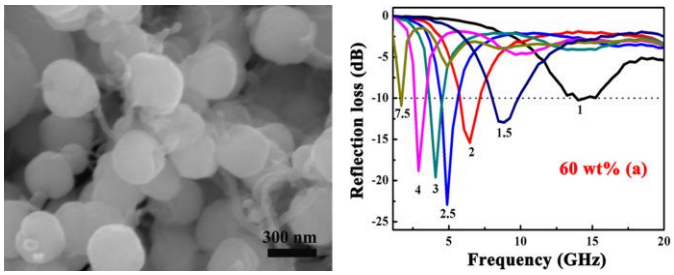

The composite structure of Co beads threaded by carbon nanotubes synthesized through a facile solvothermal method followed by a carbon reduction process exhibit superior electromagnetic wave absorption properties.